

# The Large $N$ Glueball Mass Spectrum in 2+1 Dimensions

Jesse Carlsson\* and Bruce H. J. McKellar†

*School of Physics, The University of Melbourne*

(Dated: November 21, 2018)

## Abstract

In this paper we explore the large  $N$  limit of the glueball mass spectrum for 2+1 dimensional pure gauge theory. We employ Hamiltonian lattice gauge theory (LGT) and analytic variational techniques to calculate glueball masses for finite values of  $N \leq 25$ . The results are then accurately extrapolated to infinite  $N$ . An empirical observation is discussed which links the infinite  $N$  glueball spectrum to a simple oscillator model.

---

\*Electronic address: [j.carlsson@physics.unimelb.edu.au](mailto:j.carlsson@physics.unimelb.edu.au)

†Electronic address: [b.mckellar@physics.unimelb.edu.au](mailto:b.mckellar@physics.unimelb.edu.au)

## I. INTRODUCTION

In this paper we study the glueball mass spectrum for large  $N$  pure gauge theory (no quarks) in 2+1 dimensions using Hamiltonian LGT. Our primary motivation lies in recent developments in string theory where a direct connection between pure gauge theory in the large  $N$  limit and certain string theories has been conjectured. An independent test of this conjecture is provided by large  $N$  calculations of the glueball mass spectrum in LGT. Impressive Monte Carlo calculations by Teper [1] and Lucini and Teper [2, 3] have progressed to the stage where accurate values of glueball masses have been calculated up to  $N = 6$  in 2+1 dimensions. This has allowed an extrapolation to the  $N \rightarrow \infty$  limit. With the analytic techniques of the Hamiltonian approach [4] it is possible to extend these calculations to much larger  $N$ , allowing a more reliable  $N \rightarrow \infty$  extrapolation.

The outline of this paper is as follows. We start in Section II with a historical background, where the original motivations for large  $N$  physics are discussed and the recent developments in string theory introduced. In Section III we use the analytic variational approach discussed in Ref. 4 to calculate glueball masses at finite values of  $N$  up to  $N = 25$  in some cases. These results are then extrapolated to explore the large  $N$  limit of the 2+1 dimensional glueball mass spectrum. The  $N \rightarrow \infty$  limits obtained here are compared to the results of the analogous Monte Carlo studies in the Lagrangian approach.

## II. BACKGROUND

The nonperturbative region of quantum chromodynamics (QCD) has been examined predominantly with numerical techniques. While the numerical Monte Carlo simulations of Lagrangian LGT have made significant progress, there have been few developments in analytic techniques. One analytic technique which has received considerable attention in recent years is the large  $N$  limit.

In 1974 't Hooft proposed a study of  $SU(N)$  gauge theories in the large  $N$  limit rather than the physically interesting  $N = 3$  case [5]. It was hoped that the  $SU(N)$  theory could be solved analytically and would be, in some sense, close to  $SU(3)$ . Indeed it was shown that the large  $N$  theory simplifies drastically [5] but still captures at least some of the complexity of the  $SU(3)$  theory [6, 7]. Motivated by the fact that the QCD coupling constant  $g^2$  is

a poor expansion parameter because its value depends on the energy scale of the process under consideration, 't Hooft considered an expansion in another dimensionless parameter of  $SU(N)$  QCD,  $1/N$ . Based on an ingenious organisation of Feynman diagrams, 't Hooft was able to show that in the large  $N$  limit, keeping the 't Hooft coupling  $g^2N$  fixed, only planar diagrams remain. While the remaining planar theory can be solved exactly in two dimensions, the three and four dimensional theories have not yet been solved.

Recent developments in string theories have attempted to address this problem. In 1997 Maldacena conjectured a correspondence, in the duality sense, between superconformal field theories and string theory propagating in a non-trivial geometry [8]. The idea behind duality is that a single theory may have two (or more) descriptions with the property that when one is strongly coupled the other is weakly coupled. A technique for breaking the conformal invariance and supersymmetry constraints of Maldacena's original proposal was later developed by Witten [9]. This led to the hope that nonperturbative pure  $SU(N)$  gauge theories could be described analytically in 3+1 dimensions by their string theory dual. To develop this hope into a concrete solution would require perturbative expansions within the dual string theory. Such developments would seem to be some way off.

In order to test the viability of using string theories to probe nonperturbative QCD independent tests are needed. The glueball mass spectrum of QCD provides a perfect laboratory. Recent Monte Carlo calculations have provided stable estimates of glueball masses up to  $N = 6$  [1, 3] in 2+1 dimensions and up to  $N = 5$  [3] in 3+1 dimensions. From these estimates an  $N \rightarrow \infty$  limit can be extrapolated in each case. Convincing evidence of  $\mathcal{O}(1/N^2)$  finite  $N$  corrections have been demonstrated in 2+1 dimensions, verifying a specific prediction of 't Hooft's  $1/N$  expansion in the quarkless case. From the string theory side, present calculations require a strong coupling limit ( $N, g^2N \rightarrow \infty$ ) to be taken. In this limit the string theory reduces to classical supergravity and the calculation of glueball masses,  $m(J^{PC})$ , is straightforward. In this limit the glueball is represented by a dilaton field whose mass can be extracted by solving the dilaton wave equation [10–12]. Despite the extreme approximations required surprising quantitative agreement with the weak coupling results from LGT were obtained. Later it was realised that, in 2+1 dimensions, lower mass states can be constructed from the graviton field [13]. With this approach the quantitative

agreement with LGT is lost but qualitative agreement in the form of the prediction

$$m(0^{++}) < m(2^{++}) < m(1^{-+}) \quad (1)$$

still holds. The qualitative agreement between string theories and LGT persists in 3+1 dimensions [14] with

$$m(0^{++}) < m(2^{++}) < m(0^{-+}), \quad (2)$$

for both theories. It appears that the identification of glueball states remains a problem. A serious difficulty is the removal of unwanted states which have masses of the same magnitude as the glueballs. Recipes for removing these unwanted states have been proposed [15, 16] but new parameters need to be introduced.

The exploration of large  $N$  gauge theories outside of string theory has not been restricted to traditional Monte Carlo methods. Recent studies using the light-front Hamiltonian of transverse LGT have shown agreement with the Monte Carlo calculations of Teper [17]. In this approach explicit calculations at  $N \rightarrow \infty$  are possible without the need for extrapolation. Continuum calculations, without the use of string theory, have also commenced. An impressive series of papers [18–20] has led to specific predictions for the string tension for all  $N$  in 2+1 dimensions [20]. These predictions lie within 3% of lattice calculations up to  $N = 6$  beyond which LGT results are not available. A recent review is available in Ref. 21.

### III. EXTRAPOLATION

#### A. Introduction

In this section we calculate 2+1 dimensional  $SU(N)$  glueball masses for various  $N$  using the analytic variational technique of Ref. 4. Our intention is to explore the large  $N$  limit of glueball mass spectrum by extrapolating the results obtained to their  $N \rightarrow \infty$  limit. Employing analytic methods we can extend the calculation of the lowest energy massgaps to  $SU(25)$  on a desktop computer. This should be compared to current results in the Lagrangian approach which are limited, at present, to  $SU(6)$ . With large values of  $N$  available a more reliable extrapolation to the  $N \rightarrow \infty$  limit is possible.

To simulate the ground, or (perturbed) vacuum, state with energy  $E_0$ , we use the one

plaquette trial state,

$$|\phi_0\rangle = \exp \left( c \sum_{\mathbf{x}, i < j} \text{Re} \left[ \text{Tr} \left( U_i(\mathbf{x}) U_j(\mathbf{x} + \hat{\mathbf{i}}a) U_i^\dagger(\mathbf{x} + \hat{\mathbf{j}}a) U_j^\dagger(\mathbf{x}) \right) \right] \right) |0\rangle. \quad (3)$$

Here,  $|0\rangle$  is the strong coupling vacuum defined by  $\mathcal{E}_i^\alpha(\mathbf{x})|0\rangle = 0$  for all  $i$ ,  $\mathbf{x}$  and  $\alpha = 1, 2, \dots, N^2 - 1$ .  $\mathcal{E}_i^\alpha(\mathbf{x})$  is the lattice chromoelectric field on the directed link running from the lattice site labelled by  $\mathbf{x}$  to that labelled by  $\mathbf{x} + a\hat{\mathbf{i}}$ . Here  $\hat{\mathbf{i}}$  is a unit vector in the  $i$  direction. The directed square denotes the traced ordered product of link operators,  $U_i(\mathbf{x})$ , around an elementary square, or plaquette, of the lattice,

$$\text{Tr} \left[ U_i(\mathbf{x}) U_j(\mathbf{x} + \hat{\mathbf{i}}a) U_i^\dagger(\mathbf{x} + \hat{\mathbf{j}}a) U_j^\dagger(\mathbf{x}) \right] \quad (4)$$

where  $a$  is the lattice spacing.

As discussed in Ref. 4, the precise form of  $c(\beta)$ , where  $\beta = N/g^2$ , is unimportant in a scaling region. As it turns out, to calculate variational wave functions, by minimising the vacuum energy density, for large dimension gauge groups is cumbersome. Numerical precision becomes a factor in the minimisation of the energy density. This problem is magnified in the calculation of tadpole improved results using the iterative procedure employed in Ref. 4. We thus abandon the use of variational wave functions here. Instead we make use of the one plaquette wave function of Eq. (3) and define a simple dependence of  $c(\beta)$ . Here we choose  $c(\beta) = \beta$ .

Many Hamiltonians are available for LGT calculations [22]. In Ref. 4 we used Kogut-Susskind [23], improved and tadpole improved Hamiltonians to calculate glueball masses for  $N \leq 5$ . Here we employ the simplest of these, the Kogut-Susskind Hamiltonian, which is defined for pure  $\text{SU}(N)$  gauge theory with coupling  $g^2$  on a lattice with spacing  $a$  by

$$\mathcal{H} = \frac{g^2}{2a} \sum_{\mathbf{x}, i} \mathcal{E}_i^\alpha(\mathbf{x})^2 + \frac{2N}{ag^2} \sum_{\mathbf{x}, i < j} P_{ij}(\mathbf{x}), \quad (5)$$

where the plaquette operator is given by

$$P_{ij}(\mathbf{x}) = 1 - \frac{1}{N} \text{Re} \left[ \text{Tr} \left( U_i(\mathbf{x}) U_j(\mathbf{x} + \hat{\mathbf{i}}a) U_i^\dagger(\mathbf{x} + \hat{\mathbf{j}}a) U_j^\dagger(\mathbf{x}) \right) \right]. \quad (6)$$

To evaluate the matrix elements appearing in the glueball mass calculation we use the

SU( $N$ ) generating functions derived in Ref. 4,

$$\begin{aligned} G_{\text{SU}(N)}(c, d) &= \int_{\text{SU}(N)} dU e^{c\text{Tr}U + d\text{Tr}U^\dagger} \\ &= \sum_{l=-\infty}^{\infty} \left(\frac{d}{c}\right)^{lN/2} \det \left[ I_{l+j-i} \left( 2\sqrt{cd} \right) \right]_{i \leq l, j \leq l} \end{aligned} \quad (7)$$

and

$$\begin{aligned} H_m(c, d) &= \int_{\text{SU}(N)} dU \exp \left[ c(\text{Tr}U + \text{Tr}U^\dagger) + d\text{Tr}(U^m) \right] \\ &= \sum_{l=-\infty}^{\infty} \det \left[ \sum_{k=0}^{\infty} \frac{d^k}{k!} I_{l+j-i+mk}(2c) \right]_{1 \leq i, j \leq N}. \end{aligned} \quad (8)$$

Here the quantities inside the determinant are to be interpreted as the  $(i, j)$ -th entry of an  $N \times N$  matrix.

For the minimisation process, we use the same basis of rectangular states as in Ref. 4. With this basis the states  $J^{++}$  and  $J^{--}$ , with  $J = 0$  or  $2$ , are accessible. The  $J = 2$  states require the use of a minimisation basis that contains no square states so that the excited states are invariant under rotations by  $\pi$  but not  $\pi/2$ . The dependence of the massgaps on the coupling does not change significantly as  $N$  is increased. We do however observe the appearance of what could possibly be additional low  $\beta$  scaling regions as  $N$  is increased.

## B. Convergence with $l_{\text{max}}$

In Ref. 4 the dependence of the variational parameter on the truncation of the  $l$ -sum in Eq. (7) was considered. The calculation of the variational parameter depends only on the plaquette expectation value. The dependence of the massgaps on the truncation should also be explored as their calculation incorporates additional matrix elements. We find that fast convergence is achieved as  $l_{\text{max}}$  is increased for the  $0^{++}$  massgaps. A typical example is shown in Fig. 1(a), where the massgaps are almost indistinguishable up to  $\beta = 80$  on the scale of the plot. For  $0^{--}$  the convergence is not as fast. A typical example is shown in Fig. 1(b). We find that in order to obtain convergence of the antisymmetric massgaps up to  $1/g^2 \approx 350$  for SU(25) we need a truncation of  $l_{\text{max}} = 30$ .

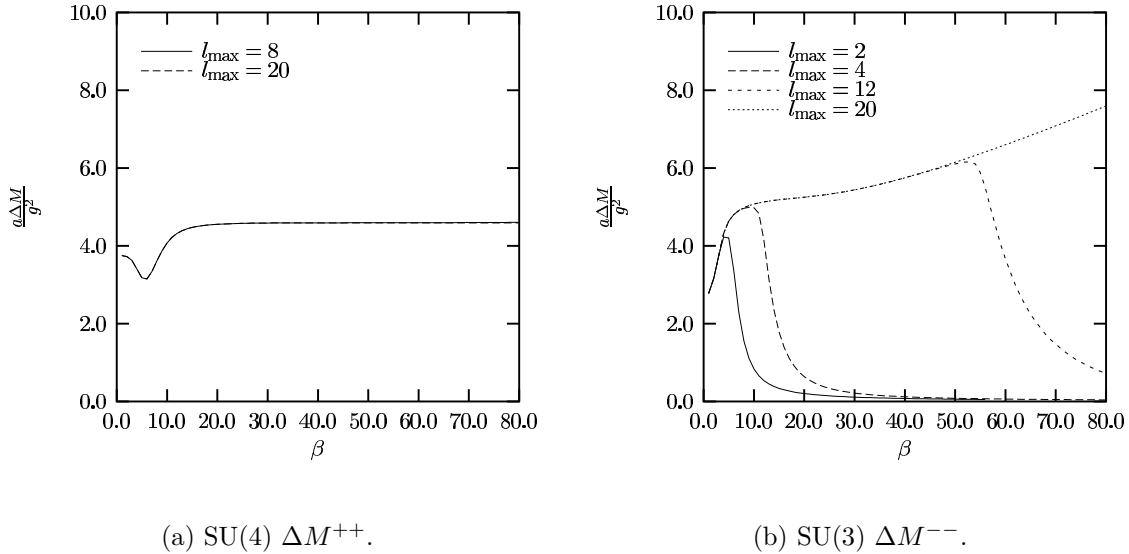


FIG. 1: Example spin 0 massgaps in units of  $g^2/a$  demonstrating different convergence properties when truncating the  $l$ -sum of Eq. (7) at  $l = \pm l_{\text{max}}$ .

### C. The small $\beta$ minima

The massgaps for  $N \geq 2$ , in units of  $Ng^2/a$  do not differ significantly as functions of  $1/g^2$ . The lowest lying  $0^{++}$  glueball masses have the characteristic form shown in Fig. 1(a) for each  $N$ . We observe a minimum at small  $\beta$  and a scaling plateau at large  $\beta$ .

In this section we examine the minima occurring in the lowest  $0^{++}$  and  $0^{--}$  glueball masses and consider the possibility that they may correspond to a scaling region. It appears that for SU(3) this region has been interpreted as a scaling region by some authors [24–26]. From the scaling arguments of Ref. 4, by changing the functional dependence of the parameter appearing in the vacuum state the scaling region can be modified. In this way it is possible to choose the variational parameter’s dependence on  $\beta$  such that the region in which the mass gap takes its minimum is stretched over a large  $\beta$  interval. In the same way, the scaling plateaux occurring for large  $\beta$  may be compressed. With this in mind, it is unclear which scaling region we should take to be the correct one. For this reason we analyse both potential scaling regions. We start, in this section, with the small  $\beta$  minima and consider the large  $\beta$  plateaux in the next section.

Fig. 2 shows the lowest lying SU( $N$ )  $0^{++}$  glueball masses in 2+1 dimensions in units of  $g^2N/a$  as functions of  $1/g^2$  for various  $N \in [3, 25]$ . It is apparent that the minima depend

only weakly on  $N$ . We see that the minima appear to approach a finite limit from below as  $N \rightarrow \infty$ . On the scale of Fig. 2 the minima corresponding to  $N = 15$  and  $N = 25$  are barely distinguishable.

Let us denote the minima in Fig. 2 by  $a\Delta M^c/(Ng^2)$  and consider them as a functions of  $N$ . Fitting  $a\Delta M^c/(Ng^2)$  to the model

$$\frac{a\Delta M^c}{Ng^2} = \gamma_1 + \frac{\gamma_2}{N^{2\gamma_3}} \quad (9)$$

for  $N \geq 8$  gives best fit parameters

$$\begin{aligned} \gamma_1 &= 0.83262 \pm 0.00022 \\ \gamma_2 &= -0.97 \pm 0.13 \\ \gamma_3 &= 0.990 \pm 0.035. \end{aligned} \quad (10)$$

We fit on the data  $N \geq 8$  to minimise pollution from next to leading order corrections. If we assert that the power of the leading order correction for finite  $N$  must be an integer power of  $1/N$ , then from Eq. (10) that order must be 2 in agreement with the predictions of large  $N$  QCD. Fitting to a model with  $1/N^2$  corrections for  $N \geq 8$  gives

$$\mu_1(N^2) = 0.83256 \pm 0.00007 - \frac{0.9753 \pm 0.0072}{N^2}. \quad (11)$$

We can go further and attempt to find the next to leading order corrections by fitting to the model

$$\frac{a\Delta M^c}{Ng^2} = \gamma_1 + \frac{\gamma_2}{N^2} + \frac{\gamma_3}{N^{2\gamma_4}}. \quad (12)$$

The best fit parameters when fit on the whole data set are

$$\gamma_1 = 0.83287 \pm 0.00011 \quad (13)$$

$$\gamma_2 = -1.116 \pm 0.028 \quad (14)$$

$$\gamma_3 = 1.715 \pm 0.085 \quad (15)$$

$$\gamma_4 = 1.627 \pm 0.050 \quad (16)$$

which is in disagreement with integer power next to leading order corrections. A good fit however is achieved to the model with  $1/N^4$  next to leading order corrections:

$$\mu_2(N^2) = 0.83233 \pm 0.00018 - \frac{0.986 \pm 0.010}{N^2} + \frac{2.772 \pm 0.090}{N^4}. \quad (17)$$

The precise locations of the minima,  $a\Delta M^c/(Ng^2)$ , are plotted as a function of  $1/N^2$  in Fig. 4 along with the fitted models of Eqs. (11) and (17).

From Eq. (11), our best fit result for the  $N \rightarrow \infty$  limit of  $a\Delta M^c/(Ng^2)$  is  $0.83256 \pm 0.00007$ . The error here is purely statistical. We should, as always, expect a significant systematic error attributable to our choice of ground state and minimisation basis. This result may be compared to the Monte Carlo calculation of Lucini and Teper who obtain the  $N \rightarrow \infty$  limit of the lowest  $0^{++}$  glueball mass as  $0.8116 \pm 0.0036$  [2]. This is comparable to the result presented here. The result of Lucini and Teper is based on a linear extrapolation to the  $N \rightarrow \infty$  limit of  $2 \leq N \leq 6$  data. Their result differs significantly from the one presented here at the leading order finite  $N$  corrections. The correction term obtained by Lucini and Teper,  $-(0.090 \pm 0.028)/N^2$ , has the same sign but is significantly smaller than the one presented here. When our data is fit on the range  $3 \leq N \leq 6$  (we don't obtain a small  $\beta$  minimum for SU(2)) our slope is halved but is still significantly larger than that of Lucini and Teper. It should be pointed out that Lucini and Teper's calculation was performed in the Lagrangian approach in which the coupling is the so called Euclidean coupling  $g_E$ . The Euclidean coupling and the Hamiltonian coupling,  $g^2$ , are equal up to order  $g_E^2$  corrections. The precise relation between the couplings is only known for small  $g_E^2$  [27], a case which does not apply for the small  $\beta$  minima. It appears that our simple calculation induces a level crossing whereby the lowest mass glueball state switches to a higher mass state beyond the small  $\beta$  minimum. Although we do not have an explanation for this, presumably, by including additional states in the minimisation basis or implementing a more complicated vacuum state, the level crossing would no longer appear and the small  $\beta$  minima would extend into large  $\beta$  scaling regions. This should be checked in further studies. A glueball mass extracted from a large  $\beta$  scaling region can be confidently compared to a corresponding Lagrangian calculation, for in that region of couplings the ratio of  $g_E^2$  to  $g^2$  is unity.

We obtain small  $\beta$  minima for the  $0^{--}$  massgaps but only for  $N \geq 5$ . Plots of these massgaps with  $N \geq 5$  are shown in Fig. 3. The behaviour is significantly different to that observed for the symmetric massgap. By  $N = 25$  the minima do not appear close to convergence. Indeed if convergence is occurring at all, it is significantly slower than was observed for the  $0^{++}$  state. To explore this further, in Fig. 5 we plot the minima of Fig. 3, which we again denote by  $a\Delta M^c/(Ng^2)$ , as a function of  $1/\sqrt{N}$ . We observe linear behaviour

in the large  $N$  limit. Fitting the  $N \geq 9$  data to the model

$$\frac{a\Delta M^c}{Ng^2} = \gamma_1 + \frac{\gamma_2}{N^{\gamma_3/2}}, \quad (18)$$

gives best fit parameters

$$\begin{aligned} \gamma_1 &= 0.41 \pm 0.01 \\ \gamma_2 &= 1.25 \pm 0.02 \\ \gamma_3 &= 0.98 \pm 0.04, \end{aligned} \quad (19)$$

which is consistent with  $\gamma_3 = 1$ . Fitting the  $N \geq 9$  data to a model with leading order finite  $N$  corrections starting at  $1/\sqrt{N}$  gives

$$\nu_1(N) = 0.41390 \pm 0.00007 + \frac{1.255 \pm 0.003}{\sqrt{N}}. \quad (20)$$

As was done for the symmetric case we can attempt to go further and find the form of the next to leading order finite  $N$  corrections. Fitting the  $N \geq 5$  data to the model

$$\nu_2(N) = \gamma_1 + \frac{\gamma_2}{\sqrt{N}} + \frac{\gamma_3}{N^{\gamma_4/2}}. \quad (21)$$

gives best fit parameters

$$\gamma_1 = 0.410 \pm 0.001 \quad (22)$$

$$\gamma_2 = 1.2718 \pm 0.0045 \quad (23)$$

$$\gamma_3 = -76 \pm 23 \quad (24)$$

$$\gamma_4 = 9.5 \pm 0.4 \quad (25)$$

indicating vanishingly small next to leading order corrections for  $N \geq 5$ . The models  $\nu_1$  and  $\nu_2$  are plotted against the  $N \geq 5$  data in Fig. 5.

The small  $\beta$  minima appear to converge to a non-zero  $N \rightarrow \infty$  limit. The convergence is significantly slower than for the small  $\beta$  minima in the symmetric case. It is also clear that the leading order finite  $N$  corrections are not the expected  $\mathcal{O}(1/N^2)$  but rather  $\mathcal{O}(1/\sqrt{N})$ . The  $N \rightarrow \infty$  limit of  $0.41 \pm 0.01$  is approximately half the corresponding  $0^{++}$  result. Such a state does not appear in the calculation of Teper.

It is possible that the small  $\beta$  minima are spurious. Dimensional analysis gives the expected scaling form but does not allow us to decide which scaling region is preferable, or

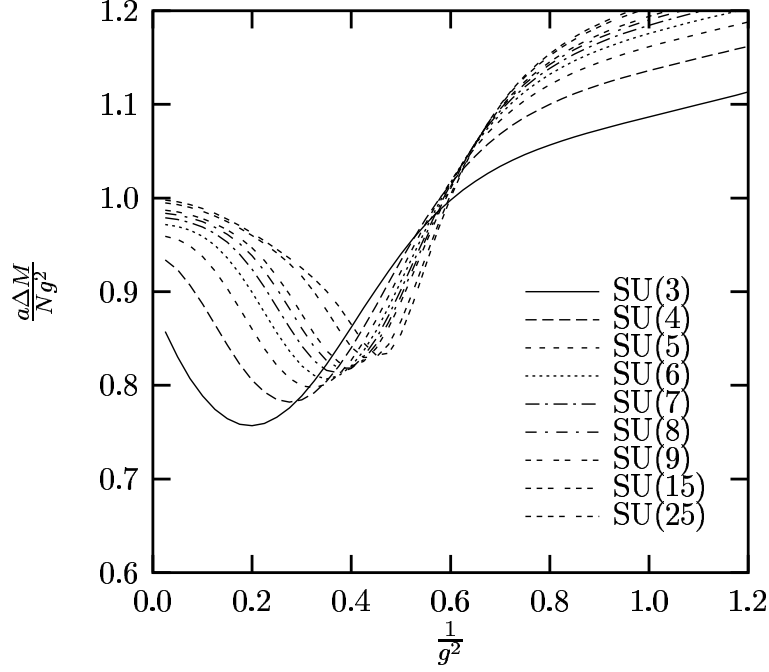


FIG. 2:  $L_{max} = 4$   $SU(N)$  lowest mass symmetric massgaps in 2+1 dimensions in units of  $g^2 N/a$  as functions of  $1/g^2$ . The  $l$ -sum of Eqs. (7) and (8) truncated at  $l_{max} = 5$ .

if one is a lattice artifact. However, based on lattice calculations to date, we expect the  $0^{++}$  glueball to be lighter than the  $0^{--}$  in the continuum limit. Spurious scaling regions have been observed in other lattice calculations [28]. It is clear that additional analysis is needed here. Again, an important step will be to include additional non-rectangular states in the minimisation basis.

#### D. The large $\beta$ plateaux

Having considered the small  $\beta$  minima as possible scaling regions we now move on to the large  $\beta$  plateaux. This scaling region appears for all  $N$  and for all states considered and so its interpretation as a genuine scaling region is less dubious. Furthermore, the glueball mass results extracted from these scaling regions may be confidently compared to the corresponding Lagrangian calculations since the ratio of the Hamiltonian to Euclidian coupling is unity up to small  $\mathcal{O}(g_E^2)$  corrections.

We start with the  $0^{++}$  state for which the best scaling behaviour is obtained. We calculate the five lowest lying massgaps corresponding to the five lowest glueball masses accessible

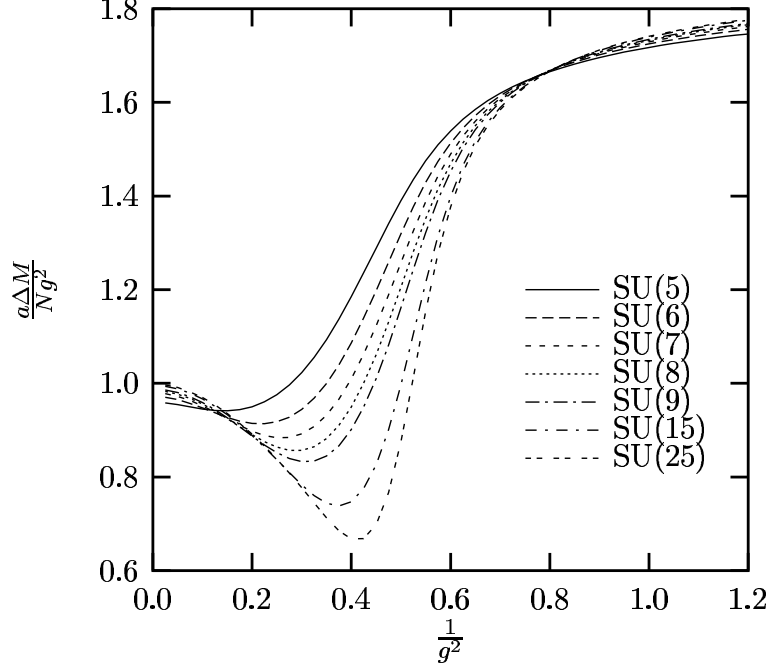


FIG. 3:  $L_{max} = 6$  SU( $N$ ) lowest mass anti-symmetric massgaps in 2+1 dimensions in units of  $g^2 N/a$  as functions of  $1/g^2$ . The  $l$ -sum of Eqs. (7) and (8) truncated at  $l_{max} = 5$ .

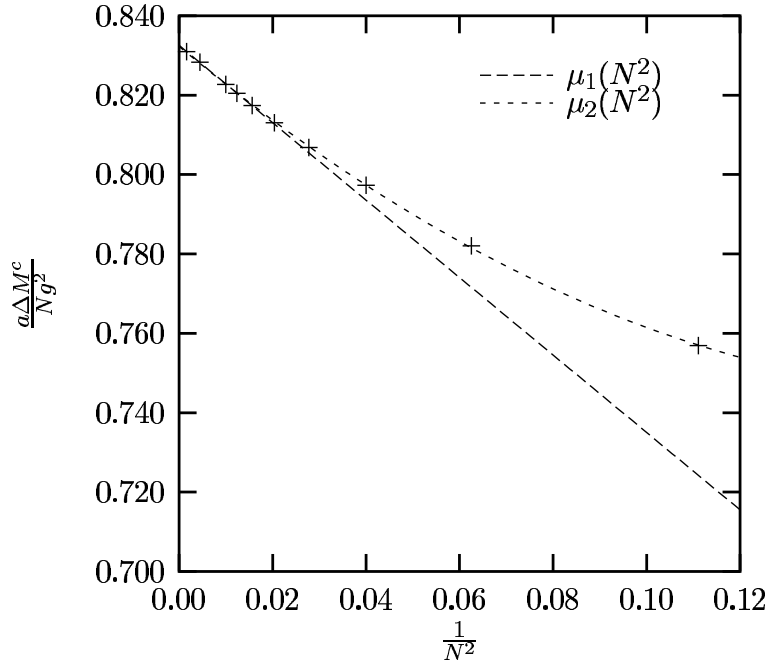


FIG. 4: The continuum limit lowest mass symmetric 2+1 dimensional massgaps in units of  $Ng^2/a$  as a function of  $1/N^2$  taken from the small  $\beta$  minima. The dashed lines are fits to Eqs. (11) and (17).

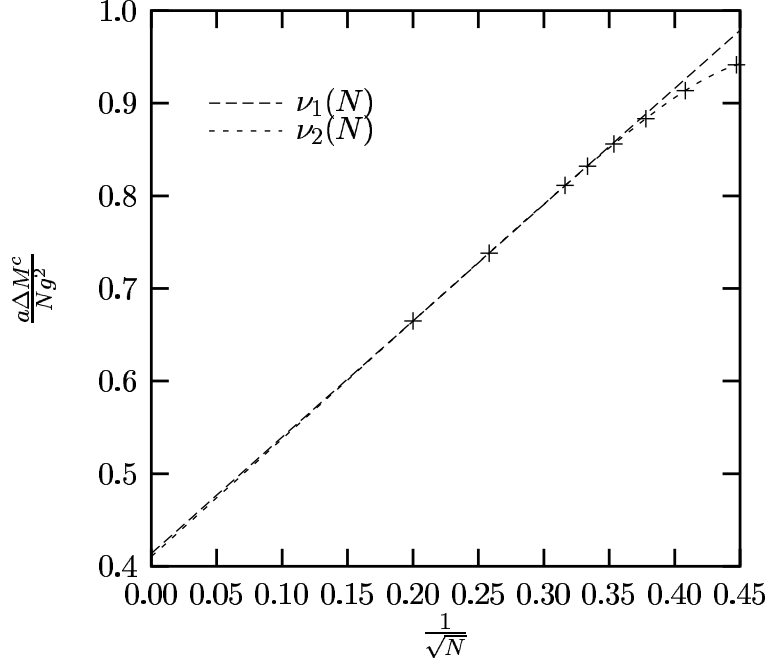


FIG. 5: The continuum limit lowest mass antisymmetric 2+1 dimensional massgaps in units of  $Ng^2/a$  as a function of  $1/\sqrt{N}$  taken from the small  $\beta$  minima. The dashed lines are fits to Eqs. (20) and (21).

with our choice of ground state and minimisation basis. We consider values of  $N$  in the range  $3 \leq N \leq 25$ . For each  $N$  considered we find a large  $\beta$  scaling plateau for each of the five lowest mass states. The lowest lying massgap is shown in Fig. 6 for a range of  $N$ . We observe that in units of  $Ng^2/a$  the massgaps do not depend strongly on  $N$  and that in the scaling region they appear to approach a finite limit. Similar observations can be made for the four higher mass states obtained although the scaling behaviour is less precise. We show the second lowest glueball mass in Fig. 7 as an example. A continuum limit for each massgap is obtained in the scaling region by fitting to a constant. For each fit we use a region of at least 10 data points which minimises the standard error. The continuum limit results for the five lowest lying massgaps, denoted by  $a\Delta M^c/(Ng^2)$ , are shown as functions of  $1/N^2$  in Figs. 6 and 9. Also shown in the plots are fits to models with leading order large  $N$  corrections starting  $1/N^2$ ,

$$\kappa_i^{++} = p_i + \frac{q_i}{N^2} + \frac{r_i}{N^4}. \quad (26)$$

Here the subscript  $i$  labels the  $i$ -th lowest glueball mass. The values of the best fit parameters are given in Table I.

TABLE I: The best fit parameters for the five lowest energy  $0^{++}$  massgaps when fitting Eq. (26) to the available data.

$i$	$p_i$	$q_i$	$r_i$
1	$1.23526 \pm 0.00023$	$-1.540 \pm 0.018$	$1.97 \pm 0.16$
2	$2.36924 \pm 0.00072$	$-2.478 \pm 0.047$	$-1.62 \pm 0.42$
3	$2.88446 \pm 0.00071$	$-3.435 \pm 0.017$	$0^a$
4	$3.35422 \pm 0.00047$	$-3.476 \pm 0.012$	$0^a$
5	$3.7667 \pm 0.0013$	$-4.114 \pm 0.092$	$1.88 \pm 0.83$

<sup>a</sup>Set to zero to obtain a stable fit.

These results should be compared with those of Lucini and Teper who obtain large  $N$  glueball masses in units of  $Ng^2/a$  in the  $0^{++}$  sector with linear fits given by

$$\begin{aligned}
0^{++} : \quad & 0.8116(36) - \frac{0.090(28)}{N^2} \\
0^{++*} : \quad & 1.227(9) - \frac{0.343(82)}{N^2} \\
0^{+++} : \quad & 1.65(4) - \frac{2.2(7)}{N^2}.
\end{aligned} \tag{27}$$

The fit for the  $0^{+++}$  state is obtained using  $4 \leq N \leq 6$  data. The remaining fits are obtained using  $2 \leq N \leq 6$  data. We find that the lowest glueball mass extracted from our large  $\beta$  plateaux is consistent, in the  $N \rightarrow \infty$  limit, with the state which Lucini and Teper label  $0^{+++}$ . The slopes of the fits are of the same sign but differ significantly in magnitude. The  $0^{+++}$  state of Lucini and Teper does not appear in our data in the form of a large  $\beta$  scaling plateau. There is however a hint of an approach to scaling in the vicinity of their result in our second lowest massgap data. This effect is only visible in our data for  $N \geq 13$  and occurs for small  $\beta$  as shown in Fig. 10. The values of  $\beta$  for which this effect appears are quite close to those for which the small beta minima are observed in the lowest mass eigenstate. Similar effects are observed in the  $0^{--}$  data but the effect is much less convincing with the data currently available.

Let us consider this small  $\beta$  region as a possible scaling region. We fit a constant to the available  $N \geq 15$  data on a range of at least 4 data points chosen so that the standard error is minimised. These scaling values are plotted as a function of  $1/N^2$  in Fig. 11. Also shown

is the best fit linear model

$$\kappa_2^{++} = 1.7605 \pm 0.0032 - \frac{5.83 \pm 0.97}{N^2}. \quad (28)$$

This produces an  $N \rightarrow \infty$  limit which is close to but inconsistent with the result obtained by Lucini and Teper for their  $0^{+++}$  state.

We now move on to the  $0^{--}$  states. For these states the scaling behaviour is not as precise as that obtained for the  $0^{++}$  states. Again we calculate the five lowest lying massgaps corresponding to the five lowest mass glueballs accessible with our choice of minimisation basis and ground state. For each  $N$  considered up to 25 we find a large  $\beta$  scaling plateau for each of the five states. The lowest lying massgap is shown in Fig. 12 for a range of  $N$ . The second lowest energy massgap is shown in Fig. 13. Considerably less data has been obtained for the  $0^{--}$  states due to the large  $l_{\max}$  required for convergence as discussed in Section III B. Despite this, the results qualitatively replicate those of the  $0^{++}$  states. We observe that in units of  $Ng^2/a$  the massgaps do not depend strongly on  $N$  and that in the scaling region they appear to approach a finite limit. Similar observations can be made for the four higher mass states although the scaling behaviour is less precise. The continuum limit values extracted are plotted as functions of  $1/N^2$  in Figs. 14 and 15. The dashed lines show fits of the continuum limit values to the model

$$\kappa_i^{--} = p_i + \frac{q_i}{N^2} + \frac{r_i}{N^4}, \quad (29)$$

with the parameters for each excited state given in Table II.

These results should be compared again with those of Lucini and Teper who obtain large  $N$  glueball masses in units of  $Ng^2/a$  in the  $0^{--}$  sector with linear fits given by

$$\begin{aligned} 0^{--} : & \quad 1.176(14) + \frac{0.14(20)}{N^2} \\ 0^{--*} : & \quad 1.535(28) - \frac{0.35(35)}{N^2} \\ 0^{---**} : & \quad 1.77(13) + \frac{0.24(161)}{N^2}. \end{aligned} \quad (30)$$

The result for  $0^{---**}$  is from Ref. 1. All fits were obtained using  $3 \leq N \leq 6$  data. The  $N \rightarrow \infty$  limit of our lowest lying massgap extracted from the large  $\beta$  plateaux is consistent with Teper's  $0^{---**}$  result.

Having considered spin 0 states we now move on to spin 2, the only other spin accessible when using a basis of rectangular states. For the case of spin 2 the scaling behaviour of

TABLE II: The best fit parameters for the five lowest energy  $0^{--}$  massgaps when fitting Eq. (29) to the available data.

$i$	$p_i$	$q_i$	$r_i$
1	$1.8896 \pm 0.0011$	$-1.829 \pm 0.068$	$6.95 \pm 0.62$
2	$2.8930 \pm 0.0044$	$-2.96 \pm 0.23$	$6.6 \pm 2.0$
3	$3.20871 \pm 0.0047$	$-3.35 \pm 0.22$	$8.8 \pm 1.9$
4	$3.83647 \pm 0.0024$	$-3.41 \pm 0.05$	$0^a$
5	$4.0759 \pm 0.0019$	$-2.45 \pm 0.12$	$-7.4 \pm 1.1$

<sup>a</sup>Set to zero to obtain a stable fit.

the massgaps is significantly worse than for spin 0. More troublesome is the fact that the convergence of the  $2^{++}$  massgaps with increasing  $l_{\max}$  is slower than the case of  $0^{--}$ . The situation for the  $2^{--}$  state is markedly better with the convergence of massgaps with increasing  $l_{\max}$  being no different to that of  $0^{++}$ . For this reason we concentrate on the  $2^{--}$  sector here.

The  $2^{--}$  states produce less precise scaling behaviour than the spin 0 states. However large  $\beta$  plateaux appear for each of the five lowest lying massgaps. We use these regions to estimate their respective continuum limits. For these states small  $\beta$  minima do not appear. The lowest lying  $2^{--}$  massgap is shown in Fig. 16 for a range of  $N$ . Once again we observe that in units of  $Ng^2/a$  the massgaps do not depend strongly on  $N$  and that in the scaling region they appear to approach a finite limit. Similar observations can be made for the four higher mass states obtained, although the scaling behaviour worsens as the mass of the state increases. The estimated continuum limit values extracted are plotted as functions of  $1/N^2$  in Figs. 17 and 18. The dashed lines show fits to the model

$$\theta_i^{--} = p_i + \frac{q_i}{N^2} + \frac{r_i}{N^4}. \quad (31)$$

The best fit parameters for each excited state are given in Table III.

Once again these results should be compared with those of Lucini and Teper who obtain large  $N$  glueball masses in units of  $Ng^2/a$  in the  $2^{--}$  sector with linear fits derived from

TABLE III: The best fit parameters for the five lowest energy  $2^{--}$  massgaps when fitting Eq. (31) to the available data.

$i$	$p_i$	$q_i$	$r_i$
1	$3.20379 \pm 0.00006$	$-2.9571 \pm 0.0032$	$5.73912 \pm 0.02585$
2	$4.07376 \pm 0.00066$	$-2.189 \pm 0.050$	$-9.46 \pm 0.43$
3	$4.96259 \pm 0.00090$	$-4.947 \pm 0.045$	$1.99 \pm 0.35$
4	$5.26717 \pm 0.00040$	$-6.221 \pm 0.031$	$15.92 \pm 0.26$
5	$5.744 \pm 0.024$	$-5.13 \pm 0.56$	$0^a$

<sup>a</sup>Set to zero to obtain a stable fit.

$3 \leq N \leq 6$  data given by

$$\begin{aligned}
2^{--} : \quad & 1.615(33) - \frac{0.10(42)}{N^2} \\
2^{--*} : \quad & 1.87(12) - \frac{0.37(200)}{N^2}.
\end{aligned} \tag{32}$$

The  $2^{--*}$  result is from Ref. 1. The  $N \rightarrow \infty$  results presented here are significantly higher. This time no correspondence between our results and those of Lucini and Teper can be obtained.

We finish this section by presenting the mass spectra obtained for the  $0^{++}$ ,  $0^{--}$  and  $2^{--}$  sectors. The results are summarised by the plots in Figs. 19—21.

### E. An empirical observation

In this subsection we present an empirical observation that could possibly be useful in the construction of simple glueball models. Since Lucini and Teper include many small area Wilson loops in their construction of excited states, we assume that they calculate the lowest few glueball states without omission. We assume the calculations presented here give higher mass glueball states. Presumably, the correct enumeration of these states is not possible without the inclusion of nonrectangular states in the minimisation basis. For example, the third lowest mass state in a given sector calculated here could be the true seventh lowest mass state. However, when our results are combined with those of Lucini and Teper an interesting empirical observation can be made. We can choose a labelling of the  $0^{++}$ ,  $0^{--}$

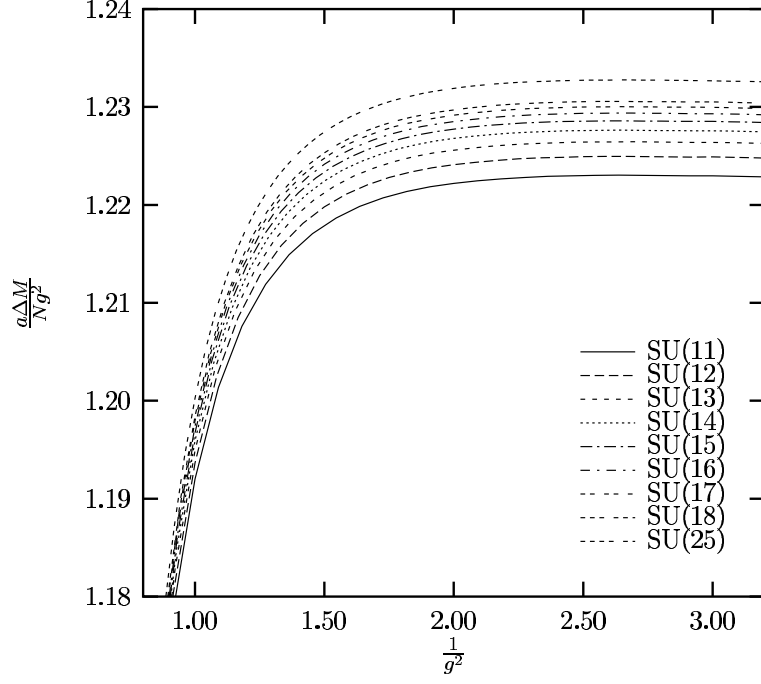


FIG. 6: Lowest mass symmetric 2+1 dimensional massgaps in units of  $Ng^2/a$  as a function of  $1/g^2$ .

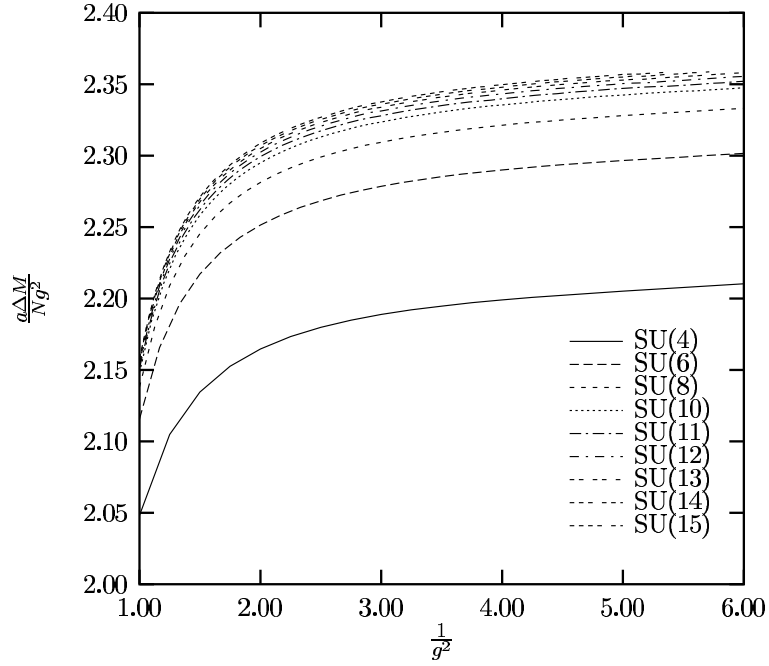


FIG. 7: Second lowest mass symmetric 2+1 dimensional massgaps in units of  $Ng^2/a$  as a function of  $1/g^2$ .

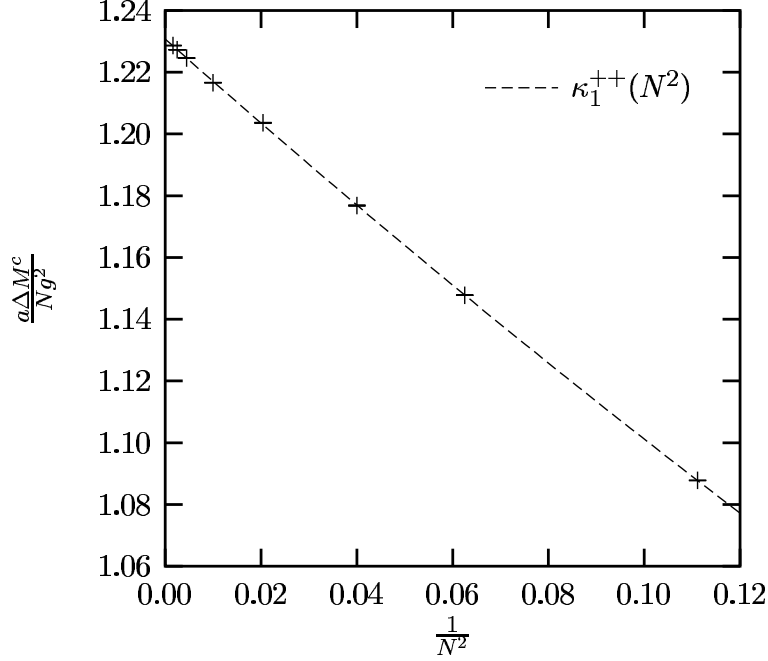


FIG. 8: Continuum limit lowest mass  $0^{++}$   $SU(N)$  massgap in units of  $Ng^2/a$  as a function of  $1/N^2$ . The dashed line is the fit to the quadratic model of Eq. (26).

and  $2^{--}$  excited states such that the large  $N$  limit of their masses lie on a straight line as shown in Fig. 22. We have included the results of Lucini and Teper for  $0^{--}$ ,  $0^{--*}$ ,  $2^{--}$  and  $2^{--*}$  which do not correspond to any of the states calculated here. The straight lines are fits to the model,

$$m_n(J^{PC}) = \gamma_1(2n + \gamma_2) \quad (33)$$

where  $\gamma_1$  and  $\gamma_2$  are parameters and  $\gamma_2$  is restricted to integer values. For the  $J^{PC}$  states considered we obtain the following best fit models

$$\begin{aligned} m_n(0^{++}) &= (0.256 \pm 0.002)(2n + 1) \\ m_n(0^{--}) &= (0.151 \pm 0.002)(2n + 5) \\ m_n(2^{--}) &= (0.1495 \pm 0.0008)(2n + 7). \end{aligned} \quad (34)$$

Here  $n \geq 1$  labels the  $n$ -th lowest mass state. We note that the fit improves in accuracy as  $n$  is increased. It is interesting to note that the slopes of the  $0^{--}$  and  $2^{--}$  models are consistent suggesting that the constant of proportionality does not depend on  $J$ . Another

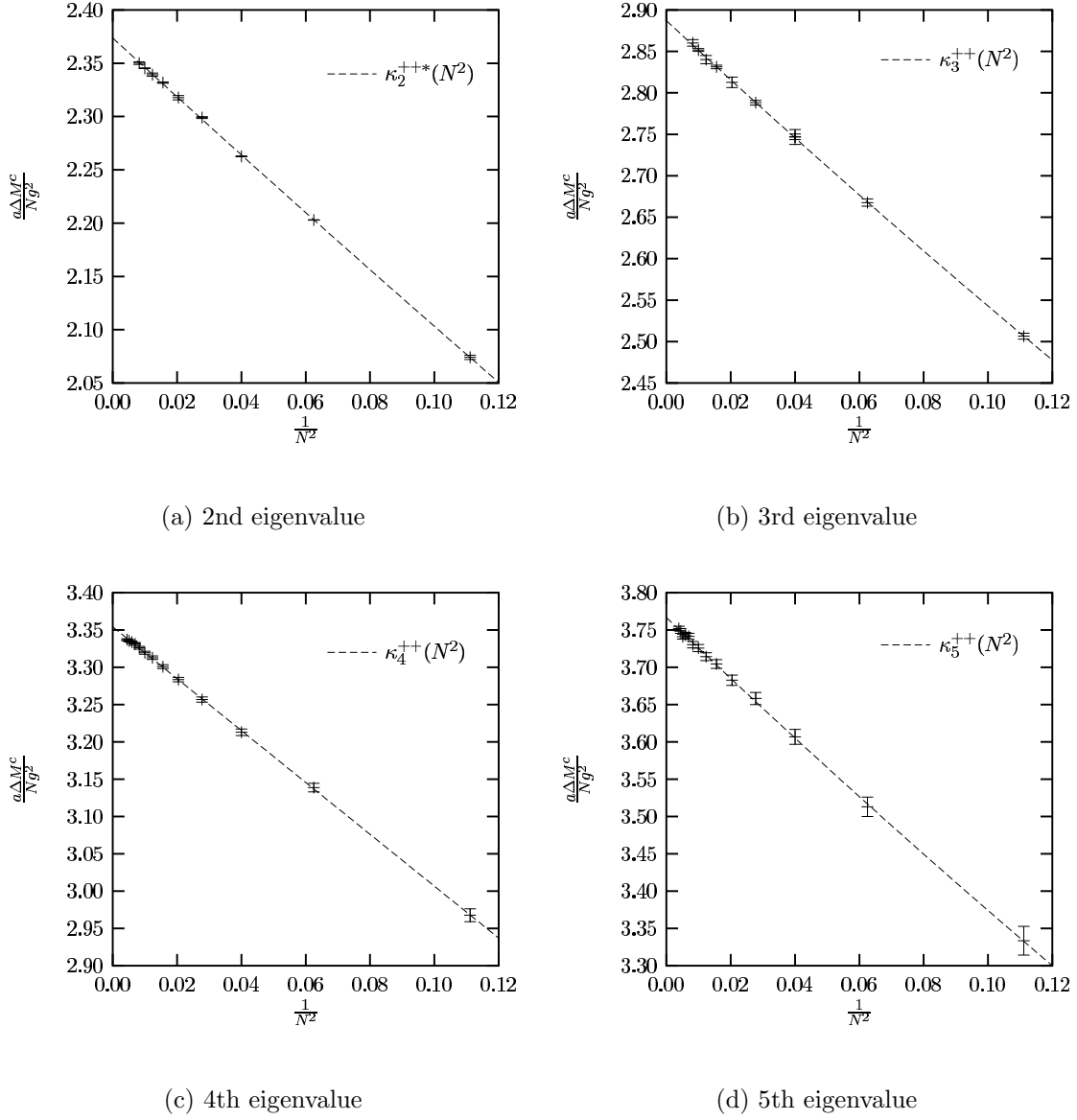


FIG. 9: Continuum limit  $0^{++}$   $SU(N)$  massgaps in units of  $Ng^2/a$  as functions of  $1/N^2$ . The dashed lines are fits given in Eq. (26).

interesting observation can be made by recasting the models in the form

$$\begin{aligned}
m_n(0^{++}) &= (0.256 \pm 0.002)(2n + 0 + 1) \\
m_n(0^{--}) &= (0.151 \pm 0.002)(2n + 4 + 1) \\
m_n(2^{--}) &= (0.1495 \pm 0.0008)(2n + 6 + 1).
\end{aligned} \tag{35}$$

We notice a similarity with the two dimensional harmonic oscillator spectrum,

$$E_n \propto 2n + J + 1, \tag{36}$$

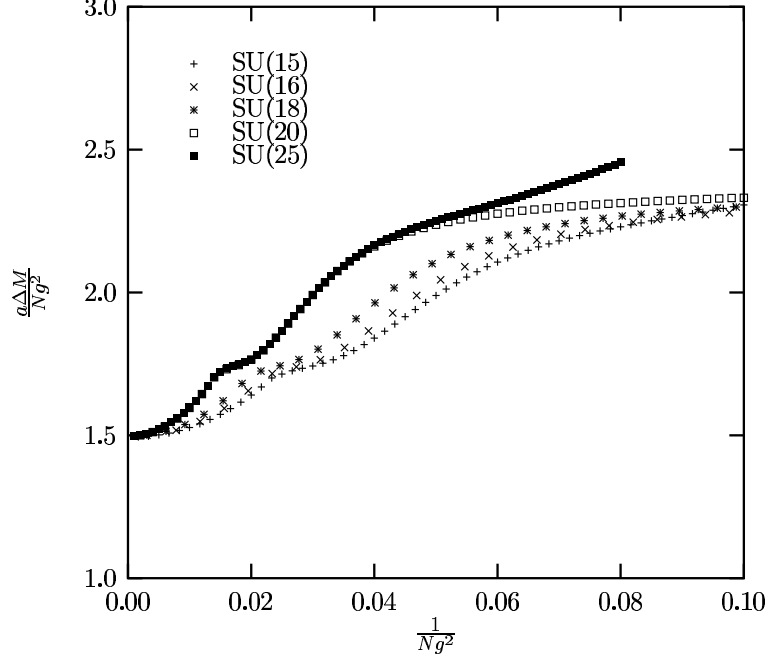


FIG. 10: Second lowest mass symmetric 2+1 dimensional massgaps in units of  $Ng^2/a$  as a function of  $1/(Ng^2)$ .

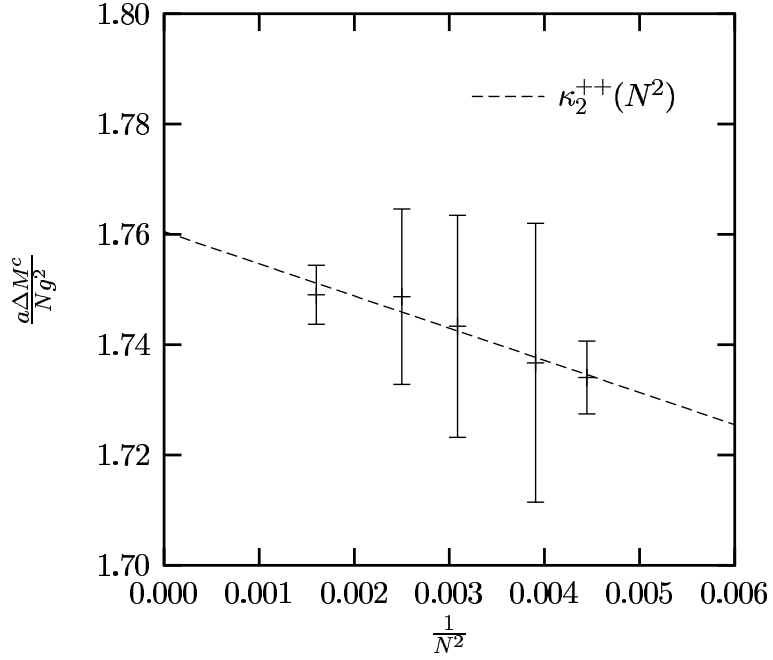


FIG. 11: Continuum limit extrapolations (in units of  $Ng^2/a$  as a function of  $1/N^2$ ) derived from the low  $\beta$  scaling region that appears for  $N \geq 13$  in the second lowest mass  $0^{++}$   $SU(N)$  massgap. The dashed line is the fit to the quadratic model of Eq. (28).

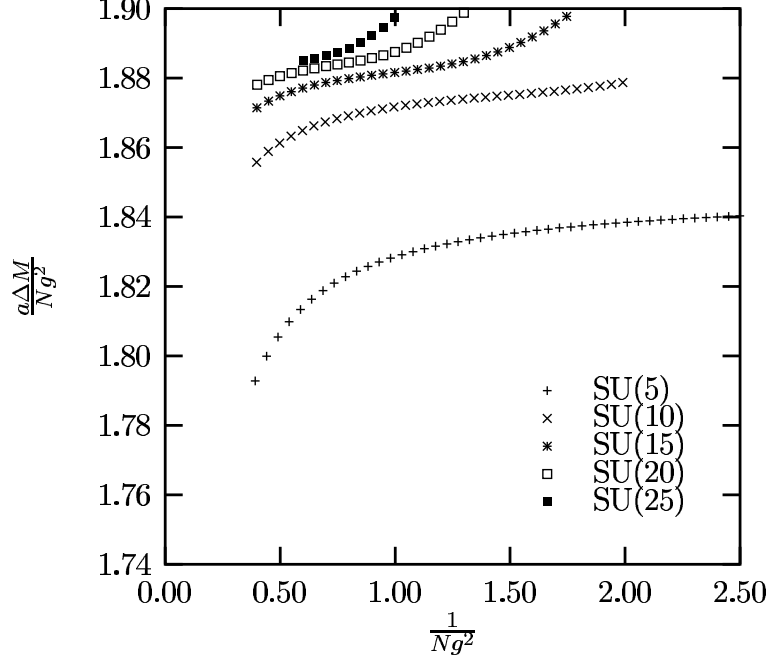


FIG. 12: Lowest mass  $0^{--}$  2+1 dimensional massgaps in units of  $Ng^2/a$  as a function of  $1/(Ng^2)$ .

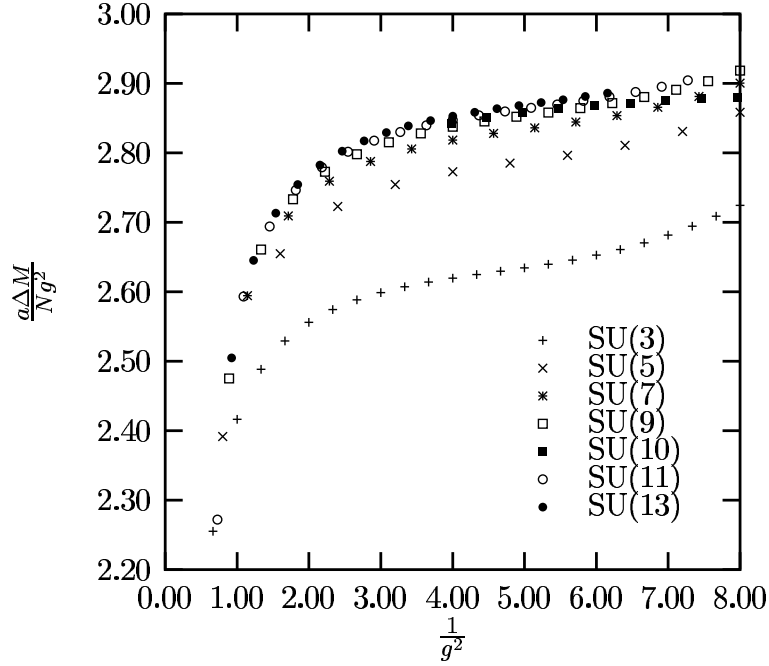


FIG. 13: Second lowest mass  $0^{--}$  2+1 dimensional massgaps in units of  $Ng^2/a$  as a function of  $1/g^2$ .

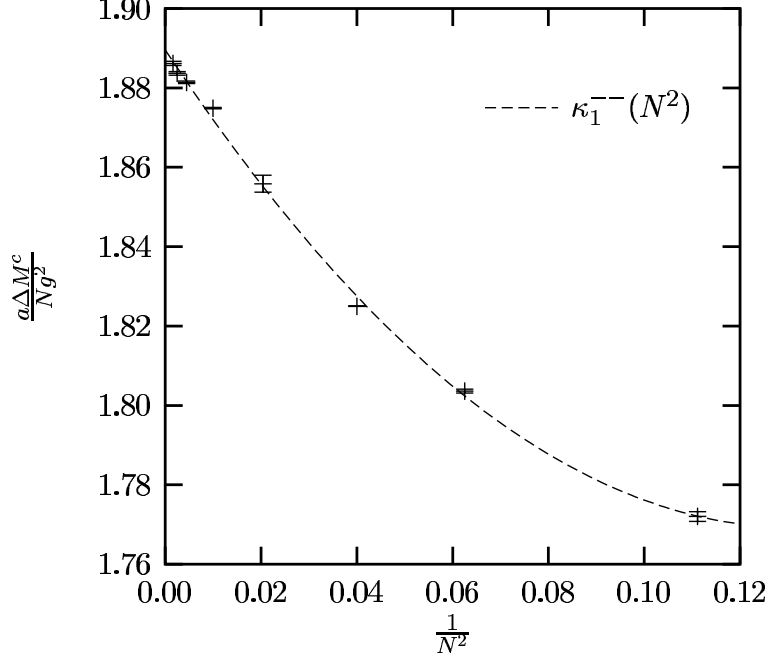


FIG. 14: The 2+1 dimensional continuum limit lowest  $0^{--}$   $SU(N)$  glueball mass in units of  $Ng^2/a$  as a function of  $1/N^2$ . The dashed line is the fit to the quadratic model of Eq. (29).

when we take into consideration the ambiguity modulo 4 of spin identification on the lattice. With this in mind we propose a simple model for the  $J^{PC}$  spectrum

$$m_n(J^{PC}) = \zeta_{PC} [2n + \gamma(J^{PC}) + 1], \quad (37)$$

where  $\zeta_{PC}$  is a spin independent parameter and  $\gamma(J^{PC})$  is an integer for which  $\gamma(J^{PC}) = J \bmod 4$ . From Eq. (34) we have  $\zeta_{--} \approx 0.15$  and  $\zeta_{++} = 0.256 \pm 0.002$ . To check this simple model we can attempt to predict the lowest lying states obtained by Lucini and Teper in the sectors that have not been considered in this paper. We start with the  $2^{++}$  sector in which Teper and Lucini obtain 1.359(12) and 1.822(62) for the  $N \rightarrow \infty$  limit of the  $2^{++}$  and  $2^{++*}$  glueball masses in units of  $Ng^2/a$ . The predictions of Eq. (37), with  $\gamma(2^{++}) = 2$  and  $\zeta_{++} = 0.256$ , are 1.28 and 1.79 for the 1st and 2nd lowest glueball masses in units of  $Ng^2/a$ . As we would expect the prediction is better for the higher mass state. We can also consider the  $1^{++}$  sector which has an equivalent spectrum to  $1^{-+}$  due to the phenomenon of parity doubling [1]. Lucini and Teper obtain 1.98(8) for the mass of the  $1^{++}$  glueball in units of  $Ng^2/a$ . The model of Eq. (37), with  $\gamma(1^{++}) = 5$  and  $\zeta_{++} = 0.256$  gives 2.048. In the  $1^{--}$  sector the agreement is not as good, with Lucini and Teper obtaining 1.85(13) for the mass of the  $1^{--}$  glueball and the model of Eq. (37), with  $\gamma(1^{--}) = 9$  and  $\zeta_{--} = 0.15$ ,

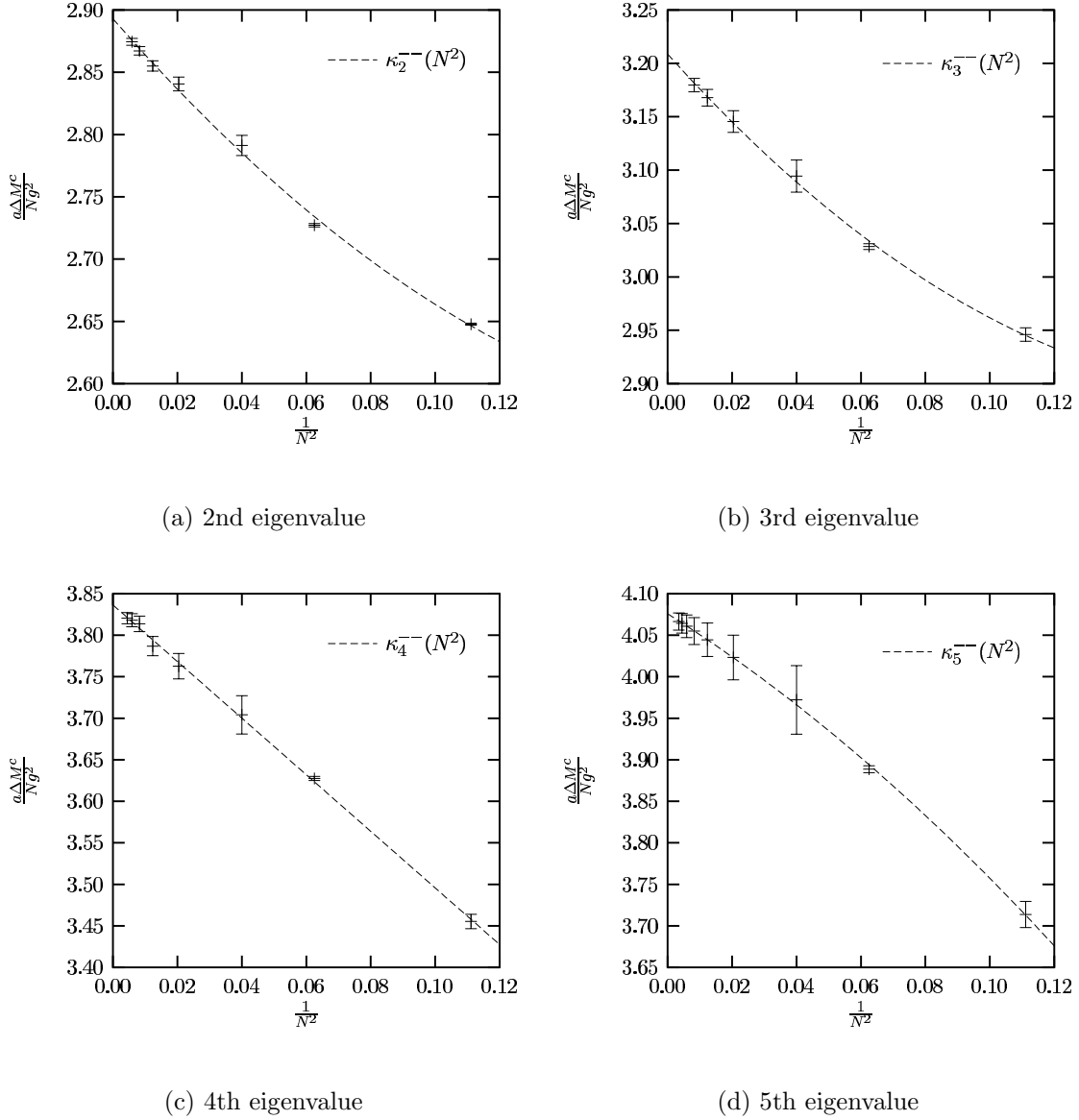


FIG. 15: Continuum limit  $0^{--}$   $SU(N)$  massgaps in units of  $Ng^2/a$  as functions of  $1/N^2$ . The dashed lines are fits given in Eq. (29).

giving 1.812.

It will be interesting to see if the model suggested here stands up to further calculations with an extended minimisation basis and in other  $J^{PC}$  sectors. The analytic techniques presented here are at a great advantage to the standard Monte Carlo techniques of Lagrangian LGT for the purpose of testing glueball models. High order excited states are readily accessible; in a variational calculation with  $s$  states in the minimisation basis,  $s$  glueball states are accessible. This is in contrast to competing Lagrangian calculations in which only 3

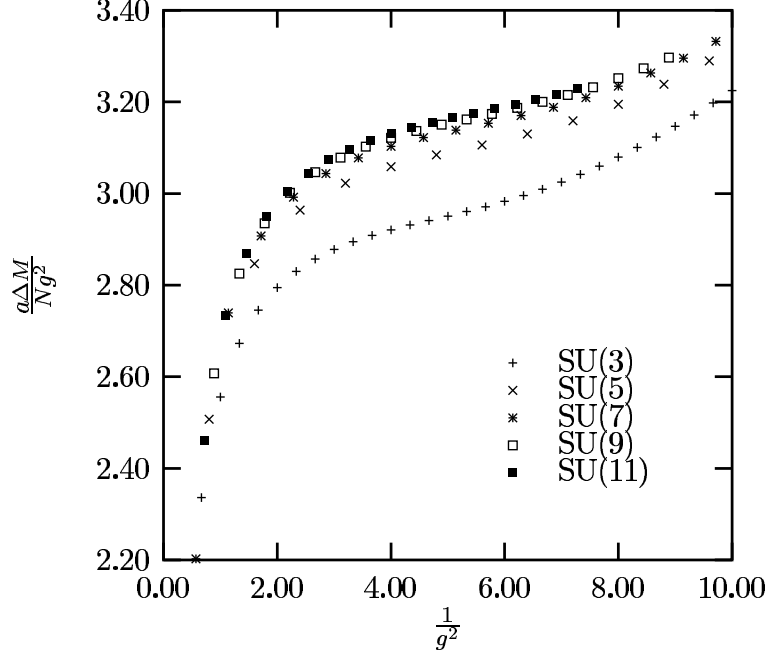


FIG. 16: The lowest lying 2+1 dimensional  $2^{--}$   $SU(N)$  massgaps in units of  $Ng^2/a$  as a function of  $1/g^2$ .

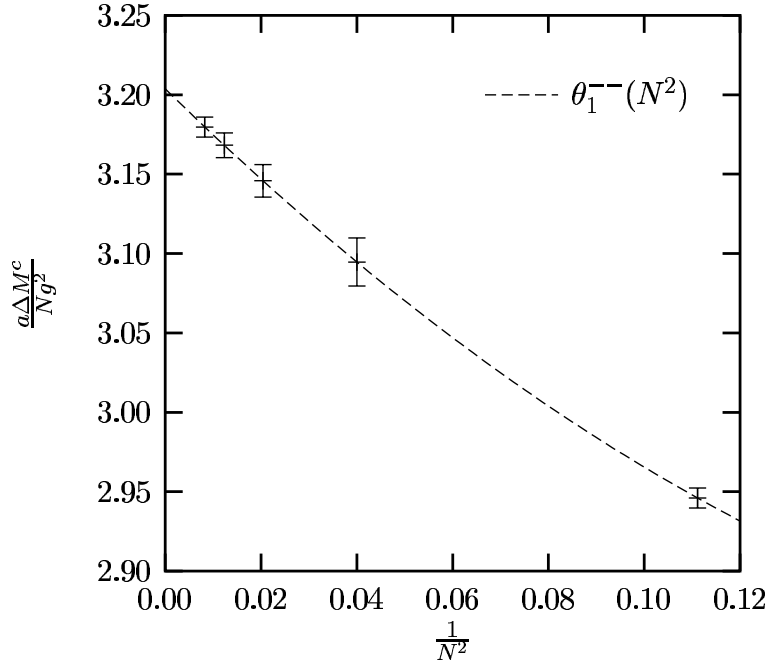


FIG. 17: The 2+1 dimensional continuum limit lowest  $2^{--}$   $SU(N)$  glueball mass in units of  $Ng^2/a$  as a function of  $1/N^2$ . The dashed line is the fit to the quadratic model of Eq. (31).

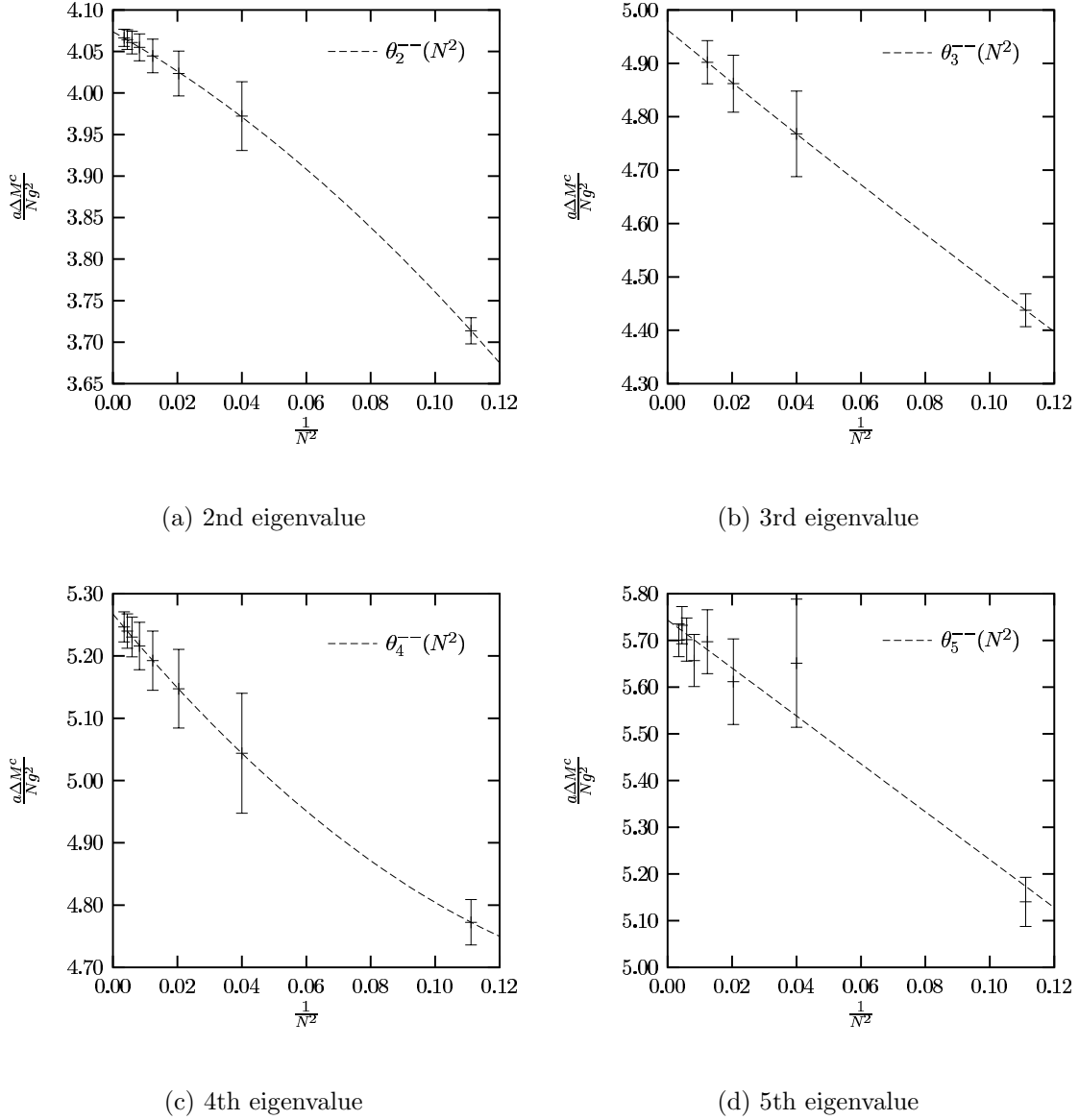


FIG. 18: The 2+1 dimensional continuum limit  $2^{--}$   $SU(N)$  massgaps in units of  $Ng^2/a$  as functions of  $1/N^2$ . The dashed lines are fits given in Eq. (31).

states are currently accessible in some  $J^{PC}$  sectors.

## F. Discussion

In this section we have calculated variational mass spectra for pure  $SU(N)$  gauge theory with a simple basis of rectangular states in 2+1 dimensions. Such a basis is easy to work with computationally and is therefore a good starting point. However to accurately explore

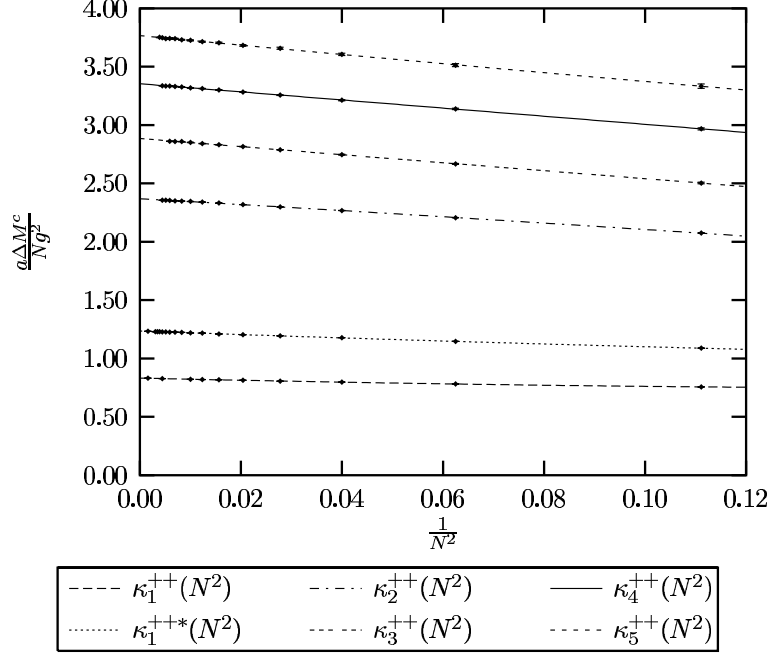


FIG. 19: An estimate of the continuum limit mass spectrum for  $0^{++}$   $SU(N)$  glueballs in units of  $Ng^2/a$  as a function of  $1/N^2$ . The lines are fits to the models of Eq. (26).

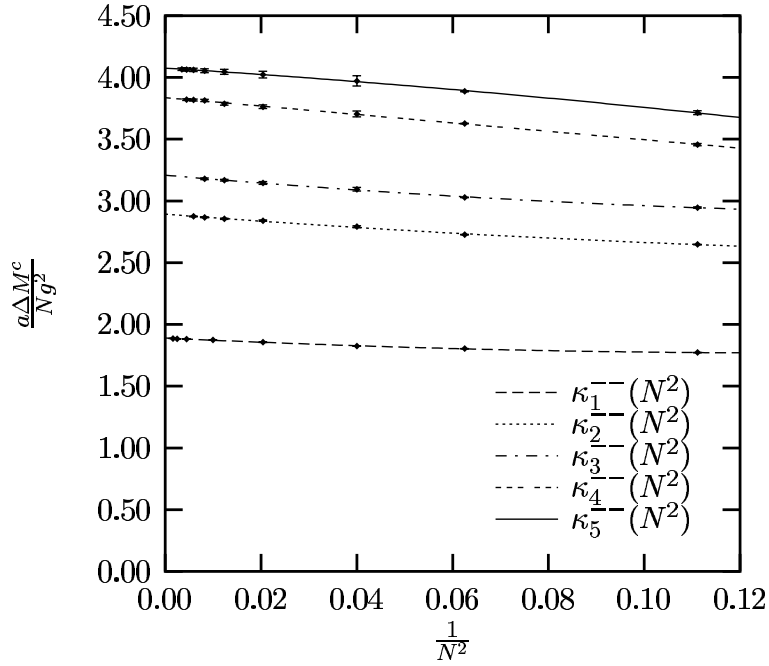


FIG. 20: An estimate of the continuum limit mass spectrum for  $0^{--}$   $SU(N)$  glueballs in units of  $Ng^2/a$  as a function of  $1/N^2$ . The lines are fits to the models of Eq. (29).

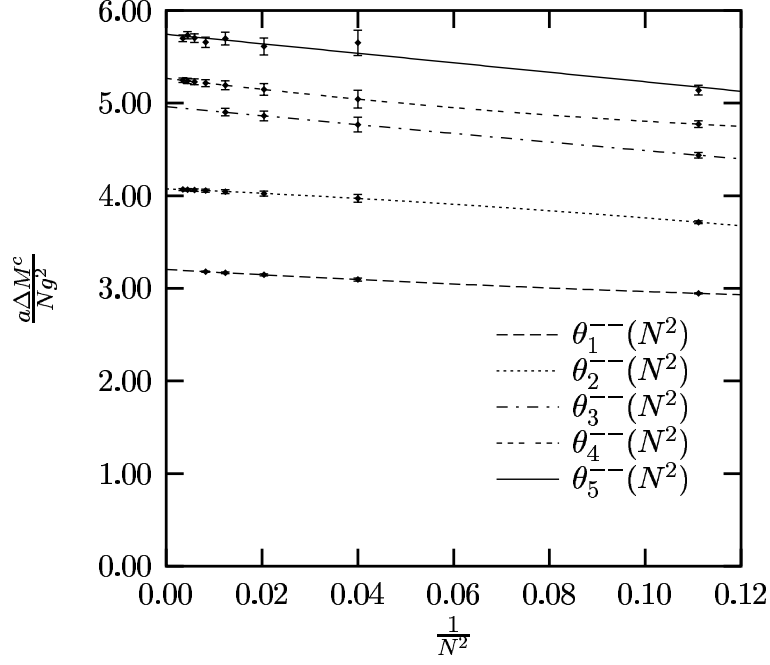


FIG. 21: An estimate of the continuum limit mass spectrum for  $2^{--}$   $SU(N)$  glueballs in units of  $Ng^2/a$  as a function of  $1/N^2$ . The lines are fits to the models of Eq. (31).

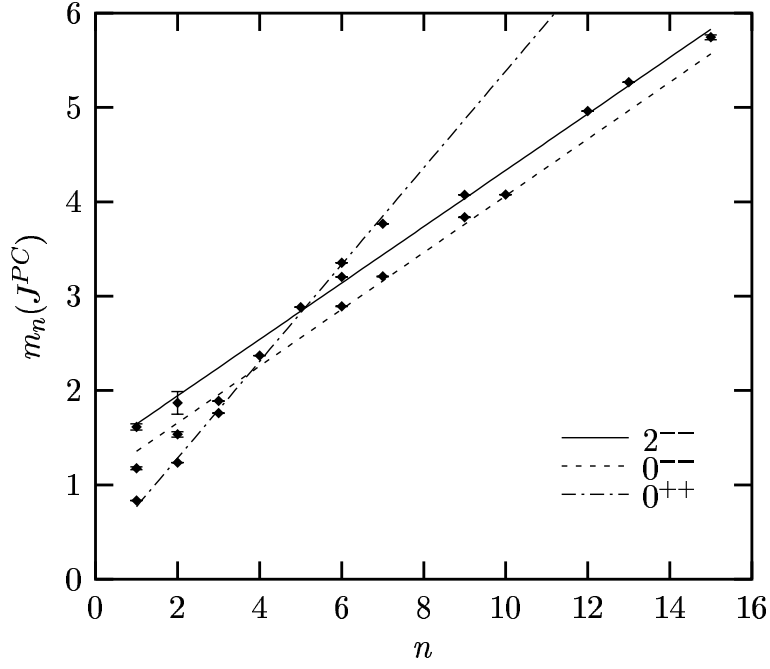


FIG. 22: A choice of enumeration of glueball masses and the fits of Eq. (35).

the pure gauge mass spectra additional states need to be included. Perhaps a more suitable basis would be the set of all states with an area less than some maximum value which would define the order of the calculation. The next stage beyond this would be to include higher representation states in the form of Wilson loops in which some links are covered more than once. In this way multiple glueball states could presumably be explored. The inclusion of additional small area states in the basis, in particular states which are not symmetric about reflections in coordinate axes, would also allow the calculation of spin 1 glueball masses and also massgaps in the  $P = -C$  sector.

It is important to point out that the inclusion of additional states in our minimisation basis does not present a significant challenge. The only complication would be in counting the possible overlaps of particular states. While more difficult than the counting required here, the process could presumably be automated using symbolic programming and techniques from graph theory. The analytic techniques used here would still be applicable until higher representation states were included in the minimisation basis. At that stage further character integrals would be required to handle the additional integrals arising in the calculation.

A final extension of the method presented here would be to make use of an improved ground state; a ground state which includes additional Wilson loops in the exponent. However, the advantage of using analytic techniques would then be lost, unless new technology was developed for tackling the resulting integrals. One would need to calculate the required matrix elements via Monte Carlo simulation on small lattices, losing the advantage of working on an infinite lattice with analytic expressions that we have here.

#### IV. CONCLUSION

In this paper we have applied the analytic techniques developed in Ref. 4, in a study of the large  $N$  glueball mass spectrum in 2+1 dimensions.

In Section III we calculated glueball masses at finite  $N$ , with  $N$  as large as 25 in some cases. This allowed accurate  $N \rightarrow \infty$  extrapolations to be made. Evidence of leading order  $1/N^2$  finite  $N$  corrections to the glueball masses was obtained, confirming a specific prediction of large  $N$  gauge theory. The interpretation of the possible scaling regions was discussed and agreement with the Lagrangian study of Lucini and Teper was obtained in some cases in the  $N \rightarrow \infty$  limit. The discrepancies are attributable to our use of only rectangular states

in the minimisation basis. Without the inclusion of small area, nonrectangular states, it is likely that some low energy states are inaccessible. Further work will fill in the incomplete spectra presented here. Interesting empirical observations were made when the results presented here were combined with those of Lucini and Teper; the enumeration of excited states can be chosen so that the glueball mass spectrum has the structure of a two dimensional harmonic oscillator. To develop this observation into a model would require a more complete calculation of the mass spectrum with nonrectangular states in the minimisation basis and possibly a more complicated vacuum trial state.

Clearly much work remains to be done before an accurate picture of the 2+1 dimensional pure  $SU(N)$  gauge theory spectrum is achieved within a Hamiltonian variational approach. We have demonstrated however that the analytic techniques of Hamiltonian LGT can be used for massgap calculations with  $N$  as large as 25 on a desktop computer. This is significantly closer to the  $N \rightarrow \infty$  limit than is currently possible with the Lagrangian approach using supercomputers. The inclusion of additional states in the minimisation basis, while not presenting a major challenge, will allow a thorough study of the 2+1 dimensional pure  $SU(N)$  mass spectrum at least up to  $N = 25$ .

### Acknowledgments

We wish to acknowledge useful and interesting discussions with J. A. L. McIntosh and L. C. L. Hollenberg.

- 
- [1] M. J. Teper, Phys. Rev. **D59**, 014512 (1999), hep-lat/9804008.
  - [2] B. Lucini and M. Teper (2002), hep-lat/0206027.
  - [3] B. Lucini and M. Teper, JHEP **06**, 050 (2001), hep-lat/0103027.
  - [4] J. Carlsson and B. H. J. McKellar (2003), hep-lat/0303016.
  - [5] G. 't Hooft, Nucl. Phys. **B72**, 461 (1974).
  - [6] E. Witten, Nucl. Phys. **B160**, 57 (1979).
  - [7] T. Eguchi and H. Kawai, Phys. Rev. Lett. **48**, 1063 (1982).
  - [8] J. M. Maldacena, Adv. Theor. Math. Phys. **2**, 231 (1998), hep-th/9711200.
  - [9] E. Witten, Adv. Theor. Math. Phys. **2**, 253 (1998), hep-th/9802150.

- [10] C. Csaki, H. Ooguri, Y. Oz, and J. Terning, JHEP **01**, 017 (1999), hep-th/9806021.
- [11] R. de Mello Koch, A. Jevicki, M. Mihailescu, and J. P. Nunes, Phys. Rev. **D58**, 105009 (1998), hep-th/9806125.
- [12] M. Zyskin, Phys. Lett. **B439**, 373 (1998), hep-th/9806128.
- [13] R. C. Brower, S. D. Mathur, and C.-I. Tan, Nucl. Phys. **B574**, 219 (2000), hep-th/9908196.
- [14] R. C. Brower, S. D. Mathur, and C.-I. Tan, Nucl. Phys. **B587**, 249 (2000), hep-th/0003115.
- [15] J. G. Russo, Nucl. Phys. **B543**, 183 (1999), hep-th/9808117.
- [16] C. Csaki, J. Russo, K. Sfetsos, and J. Terning, Phys. Rev. **D60**, 044001 (1999), hep-th/9902067.
- [17] S. Dalley and B. van de Sande, Phys. Rev. **D63**, 076004 (2001), hep-lat/0010082.
- [18] D. Karabali and V. P. Nair, Phys. Lett. **B379**, 141 (1996), hep-th/9602155.
- [19] D. Karabali, C.-J. Kim, and V. P. Nair, Nucl. Phys. **B524**, 661 (1998), hep-th/9705087.
- [20] D. Karabali, C.-J. Kim, and V. P. Nair, Phys. Lett. **B434**, 103 (1998), hep-th/9804132.
- [21] V. P. Nair, Nucl. Phys. Proc. Suppl. **108**, 194 (2002).
- [22] J. Carlsson and B. H. J. McKellar, Phys. Rev. **D64**, 094503 (2001), hep-lat/0105018.
- [23] J. B. Kogut and L. Susskind, Phys. Rev. **D11**, 395 (1975).
- [24] X.-Y. Fang, P. Hui, Q.-Z. Chen, and D. Schütte, Phys. Rev. **D65**, 114505 (2002).
- [25] Q.-Z. Chen, X.-Q. Luo, S.-H. Guo, and X.-Y. Fang, Phys. Lett. **B348**, 560 (1995), hep-ph/9502235.
- [26] C. R. Leonard, Ph.D. thesis, The University of Melbourne (2001).
- [27] C. J. Hamer, Phys. Rev. **D53**, 7316 (1996).
- [28] A. Wichmann, Ph.D. thesis, ITKP Bonn (2001).